Exploratory Research about Pneumatic Impulse De-icing Method Applied to Wind Turbine

Zhou Yu, Lichun Shu, Xingliang Jiang, Qin Hu, Hanxiang Li, Zhengfei Lei, Yuhao Liu

State Key Laboratory of Power Transmission Equipment & System Security and New Technology College of Electrical Engineering, Chongqing University, Chongqing 400044, China

yuzhoucqu@163.com, lcshu@cqu.edu.cn, xljiang@cqu.edu.cn

Abstract—**To achieve the construction of a low-carbon power system, the development speed of the wind power generation system is further improved. Wind energy is abundant at high altitudes, but wind turbines built here are easy to ice up in winter. To reduce the power loss caused by icing and ensure the stability of power dispatching, it is very important to apply anti-/de-icing methods to wind turbines. In this paper, a pneumatic impulse de-icing structure that could be applied to wind turbines is proposed. To explore the influence factors on de-icing effects of this new structure, icing and de-icing tests were carried out in an artificial climate chamber. Results show that de-icing structures with tubes made by elastic materials could peel the ice off more easily, and the de-icing effects are getting better with the increasing of tube width. In addition, with the decrease in icing temperature, the average critical de-icing pressure rises firstly and then declines, and the average de-icing area ratio is slightly affected. With the increase of ice thickness, the average critical de-icing pressure rises firstly and then declines as well. However, the average de-icing area ratio shows a reverse trend.**

Keywords— **Wind turbine, pneumatic impulse de-icing, icing, critical de-icing pressure, de-icing area ratio**

I. Introduction

As countries around the world pay more attention to energy security, ecological environment and climate change issues, accelerating the development of green energy power generation has become the international consensus to promote energy transformation and cope with global climate change. As clean and renewable energy, wind energy plays an important role in the transformation from fossil energy system to low-carbon energy system[1-2].

Wind turbines are mainly built at high altitudes, but the higher humidity and lower temperature make wind turbines more easy to ice up during winter[3]. The ice layer changes the original aerodynamic structure of blades, resulting in decreasing of lift and increasing of drag[4-5]. What's more, the uneven icing of blades will change the inherent frequency of wind turbines, resulting in unwanted vibration[6]. Therefore, it is very vital to install anti- or de-icing technologies on wind turbines working in icing areas.

At present, the main methods to prevent wind turbines from icing are divided into passive and active methods[7]. The passive methods use various paints to change the physical and chemical properties of the blade surface to reduce ice accumulation. The super-hydrophobic coating[8-9], which is the most representative passive method, can effectively delay ice accumulation. However, the hydrophobic property will be weakened as the number of icing increases[7]. The active methods mainly include thermal methods and mechanical methods. Thermal methods, including the electric heating method[10] and hot air heating method[11], have good de-icing effects but consume much time and energy[12-13]. Mechanical methods use different devices to apply external forces to the ice layer, and the ice layer will be removed by considerable normal stress or tangential stress generated by these devices. The electro impulse de-icing (EIDI) method has the advantage of high de-icing efficiency[14-15]. However, it still consumes too much energy and is at the risk of being struck by lightning. Compared with the EIDI method, the energy consumption of the pneumatic de-icing method is lower[16]. The pneumatic de-icing method was implemented on helicopter rotor blades back in the 1980s[17]. This method is to attach a tube-like flat airbag manufactured by organic polymer materials to the leading edge of aircraft wings. However, the deflection of the inflated airbag is large, usually 6mm to 10mm[18], which limits its application.

In this paper, a pneumatic impulse de-icing structure for wind turbines is proposed, and the maximal deflection is less than 3mm. To explore the de-icing effects of this new structure, icing and de-icing tests were carried out in an artificial climate chamber. According to the test results, the influences of tube parameters, icing temperature and ice thickness on the de-icing effects are obtained.

II. Design of Pneumatic Impulse De-icing Structure

A. Pneumatic Impulse De-icing Structure Sample

The test sample with pneumatic impulse de-icing structure is designed on a 400mm×80mm×20mm epoxy board, which is shown in Fig.1.

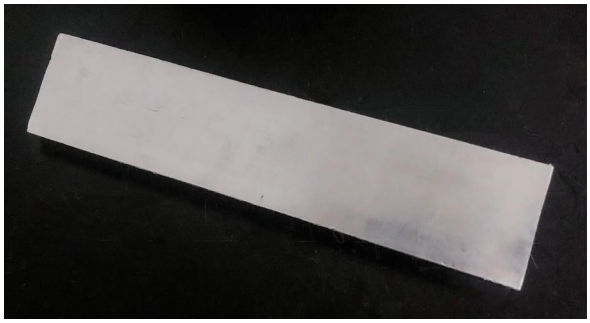

(a) Test sample

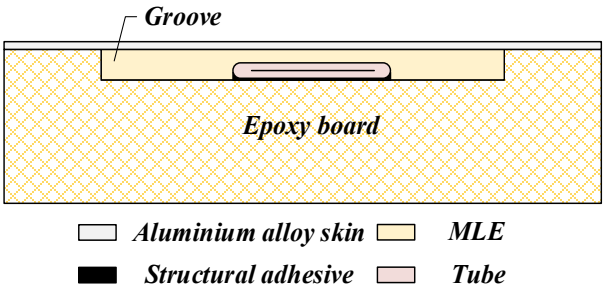

(b) The cross section of test sample

Fig.1 The diagram of test sample.

There is a 400mm×56mm×4mm groove on the top of epoxy board, on which a flat tube made by nylon material is fixed by structural adhesive. The groove will be filled with modified liquid epoxy (MLE), and after curing, the MLE becomes elastic layer with good viscosity. To protect the MLE after curing, a thin aluminium alloy skin is attached on its surface.

B. De-icing Theory of Test Sample

The operation of the test sample is given in Fig.2. When there is ice covering the aluminium alloy skin, a certain volume of pressured gas generated by the air compressor will be pumped into the tube from the inflation inlet. The tube will expand under the effect of pressured gas, leading to distortion of metal skin. When the distortion is considerable, the ice could be peeled off from the metal skin under the combined effects of bending and shear forces. The inflating process will last less than 1 second, and when the pressured gas escapes from the outlet, the metal skin will restore the initial flat state under the effect of MLE.

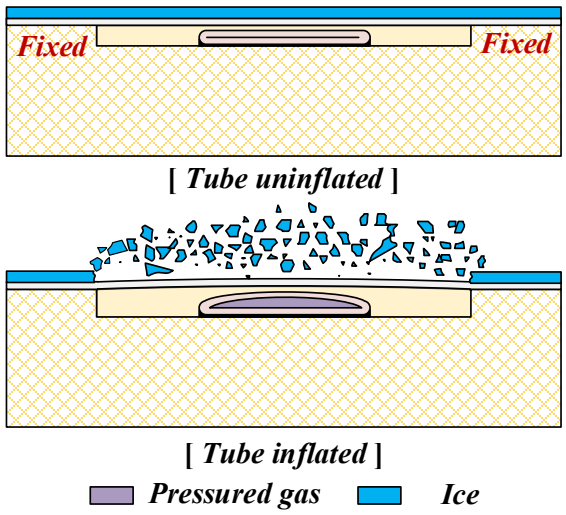

Fig.2 The operation of test sample.

The change of sample surface deflection under pressured gas could be expressed by structural dynamic equation, which is given as follow:

$$m\frac{d^2w(t)}{dt^2}+c\frac{dw(t)}{dt}+kw(t)=S(p(t)-p_0) \qquad (1)$$

where w is the surface deflection, m is the mass of the object, c is the damping coefficient, k is the elastic coefficient, S is the area that the pressured gas work on, p is the gas pressure, p_0 is the atmospheric pressure, and t is time parameter.

According to formula (1), with the increase of pressure p, the maximal surface deflection gets larger and the initial acceleration of deflection increases as well. When there is ice on the sample surface, the larger deflection will increase the bending and shear forces working on the ice layer, and the larger acceleration will make ice be peeled off by self-inertia more easily.

III. Icing and De-icing Tests

A. Test Platform

The icing and de-icing tests were carried out in the artificial climate chamber, which is shown in Fig.3. The overall length of the chamber is 3.8m, and the inner diameter is 2.0m. The temperature in the chamber is controlled by a refrigerating system with a range from -1.1 to -36℃. A spray system is installed on the ceiling in the chamber, which could provide droplet sizes from approximately 10 to 120μm. The wind is generated by a low-noise axial flow fan, which can produce wind speed up to 13m/s.

Fig.3 Artificial climate chamber.

B. Test Setting

1) *Icing Test:* Intermittent spraying is adopted during the icing tests, and the droplet size is controlled at around 40~60μm. After spraying for 3 min, the ice layer would be frozen for 15min, and repeat this process until the ice reached the wanted thickness. To explore different influence factors on de-icing effects of test samples, contrast tests are set which are given in Table I.

TABLE I. The Contrast Tests Parameters Setting

No.	Tube Material	Tube Width	Temperature	Ice Thickness
#1	elastic	2 cm	-8℃	2 mm
#2	elastic	3 cm	-8℃	2 mm
#3	elastic	4 cm	-8℃	2 mm
#4	inelastic	2 cm	-8℃	2 mm
#5	inelastic	3 cm	-8℃	2 mm
#6	inelastic	4 cm	-8℃	2 mm
#7	elastic	4 cm	-12℃	2 mm
#8	elastic	4 cm	-16℃	2 mm
#9	elastic	4 cm	-20℃	2 mm
#10	elastic	4 cm	-8℃	3 mm
#11	elastic	4 cm	-8℃	4 mm
#12	elastic	4 cm	-8℃	5 mm

2) *De-icing Test:* After the icing test, the samples would be frozen at the set temperature for half an hour before the de-icing tests. The high-pressure gas is generated by a 2.2kW air compressor and stored in a carbon fibre collecting cylinder. A high-pressure solenoid valve is used to control the inflating action. The solenoid valve is powered by a 24V DC power source. There is a point-control switch controlling the electric power supply to the solenoid valve. The mentioned facilities are shown in Fig.4.

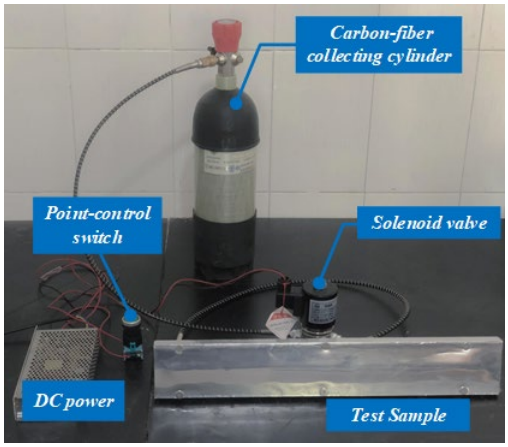

Fig.4 The de-icing facilities.

C. Parameters Measurement

1) *Measurement of Shear Stress*: As shown in Fig.5, a 5×5cm square loop is placed on 15×15cm aluminium skin used on the test sample, and there is ice frozen under the required temperature in the loop. A square pull connected with a tension meter is installed on one side of the loop. Increasing the tension slowly and recording the value of force when the ice is moved from aluminium skin and then the shear stress σ_a will be calculated as:

$$\sigma_a = \frac{F_t}{A} \tag{2}$$

where F_t is the recorded force value, A is the contact area of ice and metal skin.

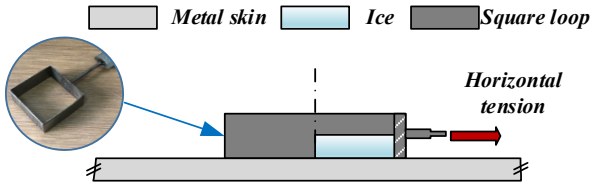

Fig.5 The diagram of shear stress measurement.

2) *Measurement of Elastic Modulus*: According to ISO 178-2010[19], the elastic modulus of ice layer under different temperatures is measured by three-point bending tests.

IV. Results

The de-icing effects are evaluated by two indicators, which are critical de-icing pressure (CDP) and de-icing area ratio (DAR). The two longer sides of aluminium skin are fixed on the epoxy board, and the width of the fixed part is 12mm. So the effective de-icing area is 400×56mm^2, which is shown in Fig.6. The DAR is the ratio of the de-icing area in the effective de-icing zone to the effective de-icing area. The lower the CDP and the larger the DAR, the better de-icing effects.

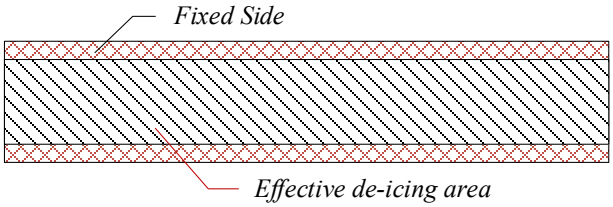

Fig.6 The diagram of effective de-icing area.

A. The Results of Shear Stress

When the ice thickness is 4mm, the relationship between shear stress and temperature is shown in Fig.7. As we can see in Fig.7, the average shear stress increases first and then decreases as the temperature goes down. When the temperature is -8℃, -12℃, -16℃ and -20℃, the average shear stress is 0.325MPa, 0.372MPa, 0.425MPa and 0.414MPa respectively.

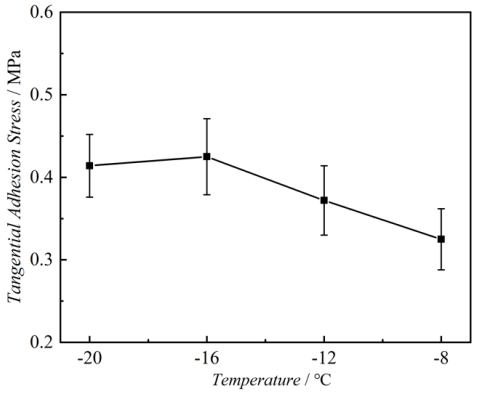

Fig.7 The relationship between shear stress and temperature.

When the temperature is -8℃, the relationship between shear stress and ice thickness is shown in Fig.8. The average shear stress increases first and then decreases as ice thickness increases. When the thickness is 2mm, 3mm, 4mm and 5mm, the average shear stress is 0.246MPa, 0.297MPa, 0.325MPa and 0.393MPa respectively.

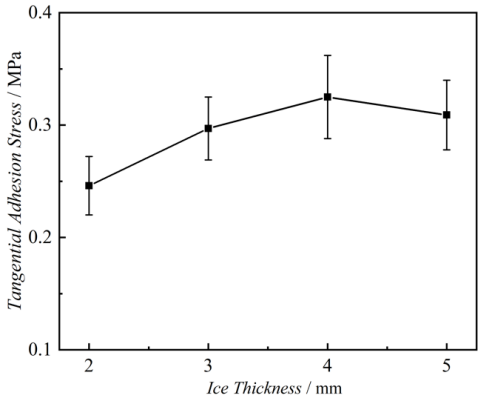

Fig.8 The relationship between shear stress and ice thickness.

B. The Results of Elastic Modulus

The average elastic modulus of ice layers under different temperatures is shown in Fig.9. As we can see in Fig.9, the maximum elastic modulus of the ice layer comes up when the temperature is -16℃, and the minimum elastic modulus

of the ice layer comes up when the temperature is -8℃. When the temperature is -8℃, -12℃, -16℃ and -20℃, the average elastic modulus is 833MPa, 1169MPa, 1421MPa and 1214MPa respectively.

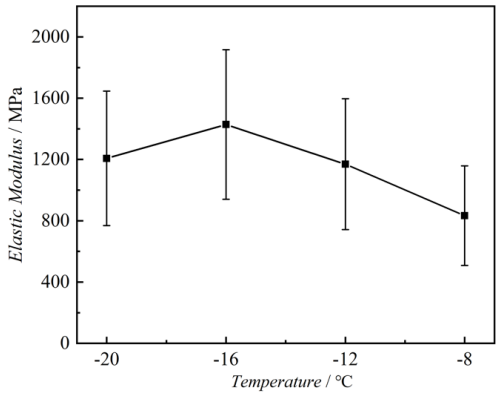

Fig.9 The elastic modulus of ice layer under different temperatures.

C. The Influences of Tube Parameters on De-icing Effects

As can be seen from Fig.10, when the tube is of the same width, the average CDP of samples using inelastic tubes are slightly larger than those using elastic tubes. This is because the elastic material is easier to deform than inelastic material under the same force (shown in Fig.11), so the samples using elastic tubes need lower pressure to generate deflection. When the tube is used in the same material, the CDP of the sample is getting lower with the increase in tube width. This is because the increasing tube width expands the stressed area of the ice layer.

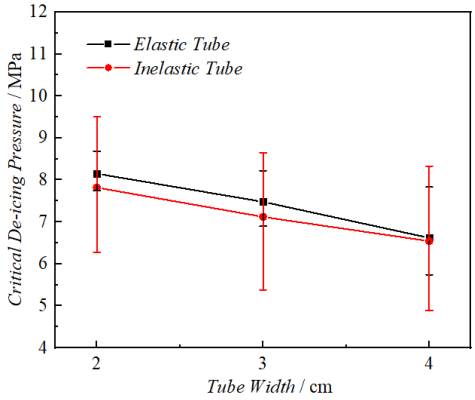

Fig.10 The CDP of samples under different tube parameters.

Fig.11 Diagram of different materials under stressed.

Fig.12 shows the results of DAR under different tube parameters. As can be seen from Fig.12, when the tube width is the same, the DAR of samples using elastic tube is larger than those using the inelastic tube. This is because the elastic tube deforms easier than the inelastic tube does. Beyond that, there are more cracks in the ice layer when using the elastic tube, which is shown in Fig.13. Under the dual effects of larger deformation and more cracks, more ice layers will fall off.

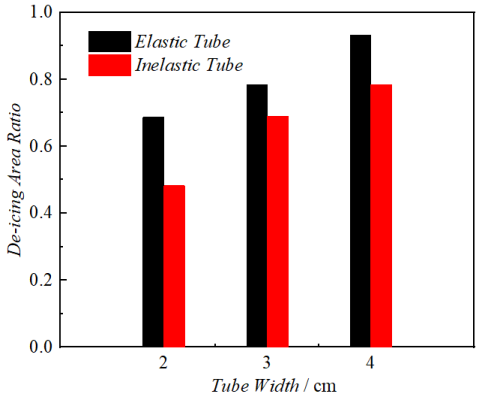

Fig.12 The DAR of samples under different tube parameters.

(a) Sample using elastic tube

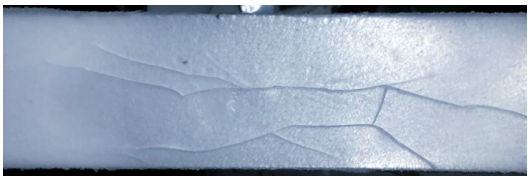

(b) Sample using inelastic tube

Fig.13 The cracks on the ice layer.

D. The Influences of Temperature on De-icing Effects

Fig.14 shows the results of de-icing effects under different icing temperatures. The most representative pictures of de-icing process under different temperatures are shown in Fig.15.

From Fig.14, it can be seen that with the decrease in temperature, the average CDP increases firstly and then decreases. This is because with the icing temperature decreasing from -8℃ to -16℃, the shear stress between the ice layer and aluminium skin is increasing. Therefore, it needs higher gas pressure to generate more deformation to peel the ice layer off. However, with the temperature decreasing further, the shear stress shows a decreasing trend. Due to this, the applied average CDP is lower. Another explanation is that, with the decreasing of icing temperature, the elastic modulus of the ice layer increases firstly and then decreases. Assume the elastomer and ice layer as a composite beam model. Based on the three-point bending test, it is found that the elastic modulus of MLE is 4 to 8 times the ice layer. So the neutral layer of the composite beam is in MLE[20]. With the increase elastic modulus of the

ice layer, the neutral layer will get close to the ice layer, and as a consequence, the shear stress on the interface between the ice layer and the metal surface will decrease.

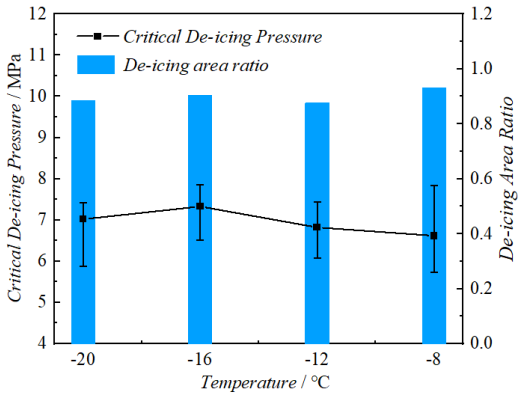

Fig.14 De-icing effects under different icing temperatures.

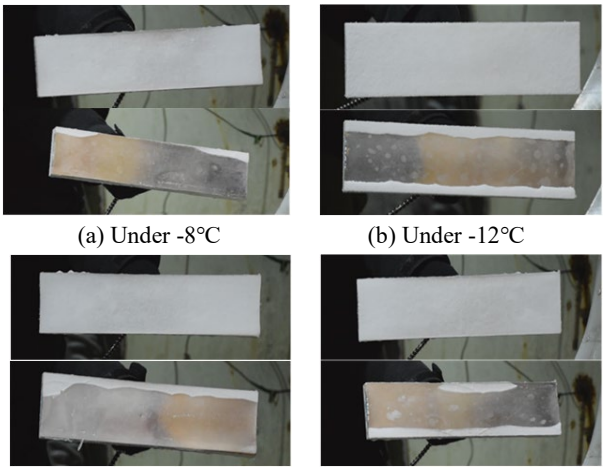

(a) Under -8℃ (b) Under -12℃

(c) Under -16℃ (d) Under -20℃

Fig.15 Pictures of de-icing tests under different temperatures.

E. The Influences of Ice Thickness on De-icing Effects

Fig.16 shows the results of de-icing effects under different ice thicknesses. The pictures of de-icing process under different ice thicknesses are shown in Fig.17.

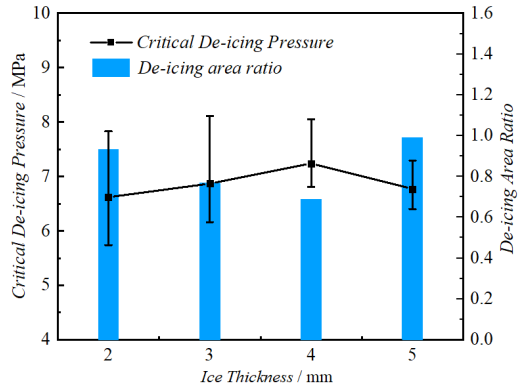

Fig.16 De-icing effects under different ice thicknesses.

From Fig.16, it can be seen that with the increase in ice thickness, the average CDP has a trend of first increasing and then decreasing. This is because as the ice thickness increases from 2mm to 4mm, the shear stress is an upward trend, and with the ice thickness increasing further, the shear stress tends to decrease. So the maximal average CDP comes up when the ice thickness is 4mm. However, the DAR has an inverse trend, and the minimal DAR comes up when the ice thickness is 4mm. As we can see in Fig.17, with the ice thickness increasing to 4mm, the de-icing area ratio is decreasing evidently.

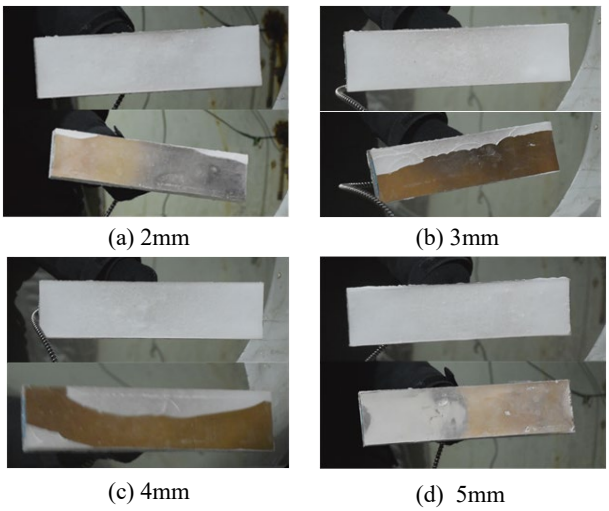

(a) 2mm (b) 3mm

(c) 4mm (d) 5mm

Fig.17 Pictures of de-icing tests under different ice thicknesses.

V. CONCLUSIONS

In this paper, a pneumatic impulse de-icing structure for wind turbines is proposed. For exploring the de-icing effects of this structure, icing and de-icing tests were carried out in artificial climate chamber. The results of the exploratory research are mainly shown as follows:

- The pneumatic impulse de-icing structure using tubes made by elastic materials has better de-icing effects. What's more, with the tube width widening, the average CDP is getting lower and the DAR is getting larger.
- With the icing temperature decreasing, the average CDP increases firstly and then decreases. The maximal average CDP come up at -16℃. In addition, there is little difference in DAR under different temperatures.
- With the icing thickness increasing, the trend of average CDP increases firstly and then decreases. However, the DAR shows a reverse trend compared with CDP. The maximal average CDP and minimal DAR come up when ice thickness is 4mm.

ACKNOWLEDGMENT

This work was supported by the National Nature Science Fund of China (Grant No.52077020 and 51977016).

REFERENCES

[1] Q. Li, W. Yu, J. Zhao, "Key Technologies for the Safe Operation of Wind and Solar Power Generation Equipment in Support of the 'Peak CO_2 Emissions and Carbon Neutrality' Policy," *High Voltage Engineering*, vol. 47, pp. 3047-3060, Sep. 2021.

[2] X. Han, T. Li, D Zhang, X. Zhou, "New Issues and Key Technologies of New Power System Planning Under Double Carbon Goals," *High Voltage Engineering*, vol. 47, pp. 3036-3046, Sep. 2021.

[3] L. Shu, Q. Gang, H. Qin, et al, "Numerical and experimental investigation of threshold de-icing heat flux of wind turbine," *Journal of Wind Engineering and Industrial Aerodynamics*, vol. 174, pp. 296-302, Mar. 2018.

[4] L. Gao, H. Hu, “Wind turbine icing characteristics and icing-induced power losses to utility-scale wind turbines,” *Proceedings of The National Academy of Sciences of The United States of America*, vol. 118, pp. 1-3, Nov. 2021.

[5] L. Shu, H. Li, Q. Hu, X. Jiang, et al, “Study of ice accretion feature and power characteristics of wind turbines at natural icing environment,” *Cold Regions Science and Technology*, vol. 147, pp. 45-54, Nov. 2018.

[6] S. Yu, D. Zhang, S. Wang, G. Wang, et al, “Field Monitoring of Offshore Wind Turbine Foundations in Ice Regions,” *Journal of Coastal Research*, vol. 104, pp. 343-350, Sep. 2020.

[7] K. Wei, Y. Yang, H. Zuo, et al, “A review on ice detection technology and ice elimination technology for wind turbine,” *Wind Energy*, vol. 3, pp. 433-457, Dec. 2019.

[8] S. Gao, B. Liu, J. Peng, et al, “Icephobic durability of branched PDMS slippage coatings co-cross linked by functionalized poss,” *ACS applied materials & interfaces*, vol. 11, pp. 4654-4666, Jan. 2019.

[9] Y. Yu, L. Chen, D. Weng, et al, “A promising self-assembly PTFE coating for effective large-scale deicing,” *Progress in Organic Coatings*, vol. 147, pp. 1-8, Oct. 2020.

[10] C. Mayer, A. Ilinca, G. Fortin, J. Perron, “Wind tunnel study of electro-thermal de-icing of wind turbine blades,” *International Journal of Offshore and Polar Engineering*, vol. 3, pp. 182-188, Jan. 2007.

[11] Y. Luo, J. Liu, Q. Chen, et al, “Research control strategy of hot air blower de-icing system for MW wind turbine blade,” *International Conference on Renewable Energy & Environmental Technology*, vol. 112, pp. 275-284, Jan. 2017.

[12] O. Parent, A. Ilinca, “Anti-icing and de-icing techniques for wind turbines: critical review,” *Cold Regions Science & Technology*, vol. 65, pp. 88-96, Jan. 2011.

[13] K. Wei, Y. Yang, H. Zuo, et al, “A review on ice detection technology and ice elimination technology for wind turbine,” *Wind Energy*, vol. 23, pp. 433-457, Dec. 2019.

[14] Y. Zhang, K. Liang, H. Lan, et al, “Modelling electro-impulse de-icing process in leading edge structure and impact fatigue life prediction of rivet holes in critical areas,” *Proceedings of the Institution of Mechanical Engineers Part G Journal of Aerospace Engineering*, vol. 234, pp. 1117-1131, Dec. 2019.

[15] X. Jiang, Y. Wang, “Studies on the electro-impulse de-icing system of aircraft,” *Aerospace*, col.6, pp. 1-15, Jun. 2019.

[16] E. Madi, K. Pope, W. Huang, T. Iqbal, “A review of integrating ice detection and mitigation for wind turbine blades,” *Renewable and Sustainable Energy Reviews*, vol. 103, pp. 269-281, Apr. 2019.

[17] J. Palacios, D. Wolfe, M. Bailey, J. Szefi, “Ice testing of a centrifugally powered pneumatic deicing system for helicopter rotor blades,” *Journal of the American Helicopter Society*, vol. 3, pp. 1-12, Jul. 2015.

[18] J. N. Weisend, “Design of an advanced pneumatic de-icer for the composite rotor blade,” in *26th Aerospace Sciences Meeting*, 1988, pp. 947-950.

[19] *Plastic - Determination of flexural properties*, International Std. 178, 2010.

[20] J. Huang, Y. Qian, H. Li, “*Stress Analysis of Superposition Beam of Different Forms*,” *Journal of Hubei University of Technology*, vol. 3, pp. 87-89, Jun. 2008.